The complex 0.1–200 keV spectrum of the Seyfert 1 Galaxy NGC 4593

M. Guainazzi[1], **G.C. Perola**[2], **G. Matt**[2], **F. Nicastro**[3,2], **L. Bassani**[4], **F. Fiore**[3,5], **D. Dal Fiume**[4], **and L. Piro**[6]

[1] Astrophysics Division, Space Science Department of ESA, ESTEC, Postbus 299, 2200 AG Noordwijk, The Netherlands
[2] Dipartimento di Fisica "E.Amaldi", Università di Roma 3, Via della Vasca Navale 84, I-00146 Roma, Italy
[3] Osservatorio Astronomico di Roma, Via dell'Osservatorio 5, I-00040 Monteporzio Catone, Italy
[4] Istituto Tecnologie e Studio Radiazioni Extraterrestri, CNR, Via Gobetti 101, I-40129 Bologna, Italy
[5] BeppoSAX Science Data Center, Via Corcolle 19, I-00131 Roma, Italy
[6] Istituto di Astrofisica Spaziale, CNR, Via Fosso del Cavaliere, I-00133 Roma, Italy

Abstract. We report on the first observation of the Seyfert 1 galaxy NGC 4593 in the 0.1–200 keV band, performed with the BeppoSAX observatory. Its spectral components are for the first time *simultaneously* measured: a power-law with photon spectral index $\Gamma \simeq 1.9$; the Compton-reflection of the primary power-law; a moderately broad ($\sigma > 60 \, \text{eV}$) K_α fluorescent line from neutral iron; and an absorption edge, whose threshold energy is consistent with K-shell photoionization from OVII. The amount of reflection and the iron line properties are consistent with both being produced in a plane-parallel, X-ray illuminated relativistic accretion disc surrounding the nuclear black hole, seen at an inclination of $\simeq 30°$. Any cutoff of the intrinsic continuum is constrained to lay above 150 keV. The claim for a strongly variable soft excess is dismissed by our data and by a reanalysis of archival ASCA and ROSAT data.

Key words: galaxies: individual: NGC 4593 – galaxies: nuclei – galaxies: Seyfert – X-rays: galaxies

1. Introduction

It is widely accepted that the huge energy output of Active Galactic Nuclei (AGN) is due to the release of gravitational energy by matter falling onto a supermassive ($\sim 10^6$–$10^8 \text{M}_\odot$) black hole. It has been known since the beginning of the X-ray astronomy that the spectrum of Seyfert 1 galaxies above a few keV and up to a few tens of keV can be described at the 0-th order by a simple power-law, with typical photon index $\Gamma \simeq 1.5$–2 (Mushotzky 1984). Later on, an emission line from neutral or mildly ionized iron (Holt et al. 1980; Perola et al. 1986; Pounds et al. 1990) and a flattening of the spectrum above $\sim 10 \, \text{keV}$ (Pounds et al. 1990; Piro et al. 1990) were discovered to be common spectral features in the class as well. Both these features have been interpreted as the effect of reprocessing of the primary radiation by optically thick matter surrounding the nucleus (George & Fabian 1991; Matt et al. 1991). The detection of the double-horned and redshifted profile of the iron line in

a long-look ASCA observation of the archetypical Seyfert 1 MCG-6-30-15 (Tanaka et al. 1995; Iwasawa et al. 1996), together with the general evidence that the iron lines are on the average broad in this class (Nandra et al. 1997), gave the first direct evidence that the reprocessing matter is located close to the black hole, probably in a Keplerian accretion disk.

In soft X-rays, an excess above the extrapolation of the high-energy power-law was measured in 50% of the Seyferts observed by EXOSAT (Turner & Pounds 1989) and about 90% of those observed by ROSAT (Turner et al. 1993; Walter & Fink 1993). The good correlation with Optical/UV (Walter & Fink 1993; Puchnarewicz et al. 1996; Laor et al. 1997) has traditionally supported the idea that this excess represents the hard tail of thermal emission from the accretion disk (Czerny & Elvis 1987), although in at least a few cases reprocessing by ionized matter seems a more viable explanation (Piro et al. 1997; Guainazzi et al. 1998b). However, caution must be employed when evaluating the soft excess in band-limited detectors and/or from multi-instrumental fits of not simultaneous observations. The extrapolation of 1–10 keV power-law fits can yield "faked" soft excesses, because the so determined spectral indices can be harder than the true one, due to the flattening contribution of the reflection component. Eventually, the discovery of absorption edges from highly ionized species of oxygen in almost 50% of the Seyfert 1s observed by ASCA so far (Reynolds 1997; George et al. 1998) has suggested that in some cases the apparent soft excess could be simply due to a mis-fit of a complex and ionized absorber.

Given the spectral complexity outlined above a detailed and self-consistent description of the X-ray spectra of Seyfert 1s requires broadband spectral observations. Moreover, the various spectral components are expected to be produced in different physical regions (see Mushotzky et al. 1993 for a review of the pre-ASCA interpretative scenario, which is still largely valid) and are therefore expected to exhibit different variability patterns and/or a delayed response to the changes of the nuclear radiation flux. The simultaneous measure of all the spectral components is a crucial requirement for any X-ray observation of Seyfert galaxies (see the discussion in Cappi et al. 1996 about the dependence of the iron line measurements on the underly-

---

Send offprint requests to: M. Guainazzi (mguainaz@astro.estec.esa.nl)

ing continuum determination). The Italian-Dutch satellite Bep-poSAX (Boella et al. 1997a) carries a scientific payload which covers the unprecedented wide energy band between 0.1 and 200 keV, with imaging capabilities and good energy resolution in the 0.1–10 keV band. A program of spectral survey of a size-able sample of Seyfert 1 galaxies is ongoing, and in this *paper* we report the results of the observation of NGC 4593.

NGC 4593 ($\alpha_{2000} = 12^{\mathrm{h}}39^{\mathrm{m}}39^{\mathrm{s}}.4$, $\delta_{2000} = -5°20'39''$) is a nearby (z = 0.009) barred spiral galaxy of Hubble type SBb, which hosts a Seyfert 1 nucleus. The Spectral Energy Distri-bution (SED) is characterized by a very weak or missing "blue bump" (Santos–Lleó et al. 1994). In X–rays, the source is vari-able, on timescales of weeks-months, by a factor of ~ 3 in the in-termediate (*i.e.*: 2–10 keV) and ~ 4–5 in the soft X–rays (Ghosh & Soundararajaperumal 1993). In NGC 4593 a soft excess above the extrapolation of the intermediate X–ray power-law was ob-served both by EXOSAT (Ghosh & Soundararajaperumal 1993; Santos–Lleó at al. 1995) and ROSAT (Walter & Fink 1993). It was claimed to be variable, ranging from 0 to $\simeq 270\%$ of the intermediate X–ray extrapolated flux. However, this picture is further complicated by the ASCA discovery of a warm absorber (Reynolds 1997), with optical depths of the OVII and OVIII pho-toionization edges equal to $\simeq 0.3$ and 0.1, respectively. There was no significant evidence of broadening of a weak (Equiv-alent Width EW $\simeq 90$ eV) fluorescent line from neutral iron (centroid energy $E_c \simeq 6.35$ keV) in the ASCA data (Nandra et al. 1997). In the hard X-ray regime, BATSE measured a 20–100 keV flux of $(9.8 \pm 1.6) \times 10^{-11}$ erg cm^{-2} s^{-1} (Malizia et al. 1997), whereas the 50–150 keV OSSE 2-σ upper limit was 4.4×10^{-11} erg cm^{-2} s^{-1} (Johnson et al. 1993).

This *paper* is organized as follows. In Sect. 2 we describe the data reduction and preparation. Sect. 3 and 4 deal with the timing and spectral analysis of BeppoSAX data, respectively. In Sect. 5, we compare our findings with a reanalysis of archival ASCA data of the same object. The results are discussed in Sect. 6.

2. Data reduction

The Italian-Dutch satellite BeppoSAX carries four co-aligned Narrow Field Instruments. Two of them are gas scintillation proportional counters with imaging capabilities: the Low En-ergy Concentrator Spectrometer (LECS, 0.1–10 keV, Parmar et al. 1997) and the Medium Energy Concentrator Spectrome-ter (MECS, 1.8–10.5 keV, Boella et al. 1997b). The other two instruments are direct-view detectors, seen through a rocking collimator to achieve a continuous monitoring of the back-ground: the High Pressure Gas Scintillator Proportional Counter (HPGSPC, 4–120 keV, Manzo et al. 1997) and the Phoswitch Detector System (PDS, 13–200 keV, Frontera et al. 1997). The HPGSPC is tuned for spectroscopy of very bright sources with good energy resolution, while the PDS possesses an unprece-dented sensitivity in its energy bandpass. Only LECS, MECS and PDS data will be considered in this *paper*. The HPGSPC data points could not in fact provide significant constraints on the spectral shape of NGC 4593.

NGC 4593 was observed by BeppoSAX from 1997 Decem-ber 31 05:30:18 UT to 1998 January 2 07:10:17 UT. Data were telemetred in direct modes for all instruments, which provide full information about the arrival time, energy, burst length/rise time (RT) and, when available, position for each photon. Stan-dard reduction procedures and screening criteria have been adopted to produce linearized and equalized event files. In par-ticular, time intervals have been excluded from the scientific product accumulation when: the angle between the pointing di-rection and the Earth's limb was $< 5°$; the momentum associ-ated to Geomagnetic Cutoff Rigidity was > 6 GeV/c; the satel-lite passed through the South Atlantic Geomagnetic Anomaly (SAGA). The PDS data have been further screened by eliminat-ing 5 minutes after any SAGA passage to avoid gain instabilities due to the recovery to the nominal voltage value after instru-mental switch-on. The RT selection has been performed using crystal temperature dependent thresholds (instead of the fixed thresholds in the standard processing). Total exposure times were 31426 s, 84195 s, and 38467 s for the LECS, MECS and PDS, respectively.

Spectra of the imaging instruments have been extracted from circular regions of radius $8'$ and $6'$ around the apparent cen-troid of the source for the LECS and MECS, respectively. The background subtraction has been performed using spectra ex-tracted from blank sky event files in the same region as the source. The background contributes 5% and 3% to the LECS and MECS count rates in the relevant energy band passes. PDS background-subtracted products (spectra and light curves) have been produced by plain subtraction of the "off-" from the "on-source" products. Total net count rates were 0.310 ± 0.003 s^{-1}, 0.350 ± 0.002 s^{-1} and 0.80 ± 0.04 s^{-1} in the LECS, MECS and PDS, respectively.

In this *paper*: errors are quoted at 90% level of confidence for two interesting parameters ($\Delta\chi^2 = 4.61$, Lampton et al. 1976); energies are in the source rest frame; the cosmological parameters $q_0 = 0.5$ and $H_0 = 50$ km s^{-1} Mpc^{-1} are assumed, unless otherwise specified.

3. Timing analysis

NGC 4593 is well known to display rapid fluctuations in X-rays, with two-folding time $\simeq 1.1$ h (Barr et al. 1987). The count rates in the BeppoSAX instruments span indeed a dynamical range of about a factor of 2 on timescales as low as 3×10^4 s. We have therefore extensively searched for spectral variability associ-ated with the flux changes, extracting light curves and Hardness Ratios (HR) in different energy bands and with various binning times. In Figs. 1 and 2 we show the light curves in the 0.7–3 keV, 3–10 keV and 13–200 keV with the corresponding contiguous HR. The bands have been chosen in order to sample energy inter-vals where different spectral components dominate, see Sect. 4. In particular, the softer band is affected by the warm absorber, which is basically transparent for photons of energy higher than 3 keV. No significant variability of the HR is detected. If a fit with a constant is performed on the 3–10 keV vs. 0.7–3 keV HR, the χ^2 is 29.3 for 38 degrees of freedom (dof). The same
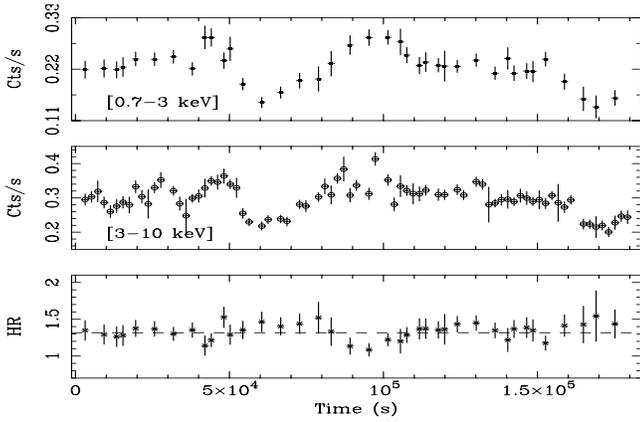
Fig. 1. Light curves in the 0.7–3 keV (LECS, *upper panel*) and 3–10 keV (MECS, *central panel*) energy bands and the corresponding HR (*lower panel*). The binning time is 2048 s. The light curves are not background-subtracted
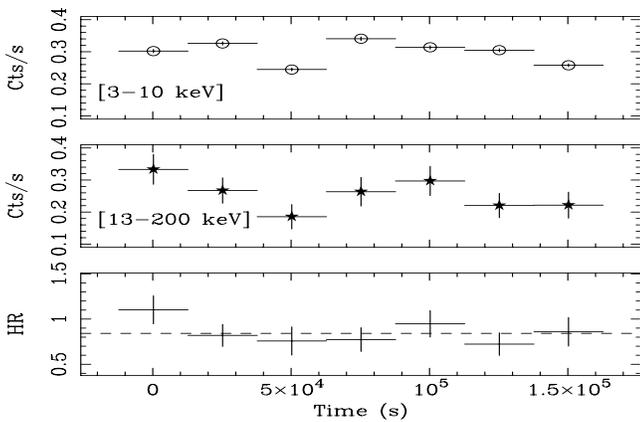

Fig. 2. Light curves in the 3–10 keV (MECS. *upper panel*), 13–200 keV (PDS, *central panel*) energy bands and the corresponding HR (*lower panel*). The binning time is 25000 s. The MECS light curve is not background-subtracted

quantity for the 13–200 keV vs. 3–10 keV HR is 4.8/6 dof. A tiny perturbation of the intermediate X-ray flux in a 2×10^4 s interval around 9×10^4 s after the beginning of the observation is not accompanied by a similar phenomenology in the soft X–rays and yields therefore a decrease of the HR by a factor $\simeq 15\%$. However, no variation in the spectral parameters above the statistical uncertainties has been detected in time-resolved spectroscopy (assuming the baseline model of Sect. 4.1). Similar results are obtained if the bands 0.1–3 and 3–10 keV are considered (see Fig. 3). We will therefore focus in the following on the time-averaged spectral behavior.

4. Spectral analysis

The spectra of the imaging instruments have been rebinned in order to sample the intrinsic energy resolution of the detectors with 3 (LECS) or 4 (MECS) energy channels. Each channel has at least 30 counts, which ensures the applicability of χ^2 test. The PDS spectrum has been quasi-logarithmically rebinned, in
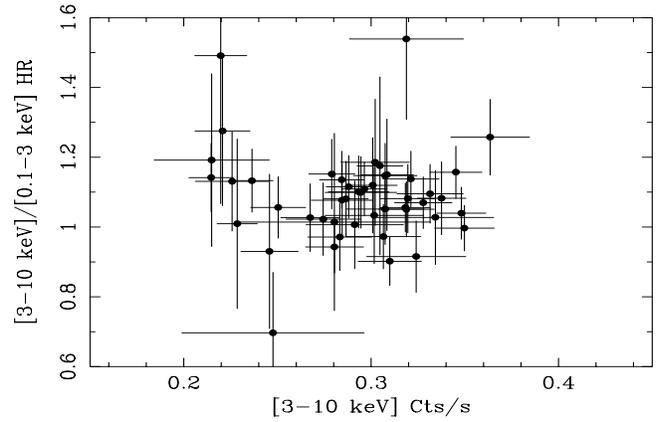

Fig. 3. 0.1–3 vs. 3–10 keV HR versus the 3–10 keV count rate. Each data point corresponds to a 2048 s light curve bin

order to have 16 energy channels in the 14–200 keV band. The spectra of the three detectors have been fitted simultaneously. Numerical relative normalization factors among the BeppoSAX instruments have been added to all the following spectral fits. The reasons is two-fold: a) the BeppoSAX instrument response matrices employed in this *paper* (September 1997 release) exhibit slight mismatches in the absolute flux calibration; b) the sampling of the instruments is not strictly simultaneous, due to the need for operating the LECS only during satellite nights or the different data selection criteria between imaging instruments and the PDS. This can affect the flux measured in variable sources as NGC 4593. The LECS to MECS factor has been left free in the fitting procedure, and turns out to be comprised in the range 0.74–0.76, which is consistent with typical values observed so far (0.7–1.1: Grandi et al. 1997; Haardt et al. 1998; Cusumano et al. 1998). The PDS to MECS factor has been instead held fixed to 0.8, as the available statistics was not good enough to provide independent constraints on it. This value corresponds to the multiplication of the best fiducial value estimated by Cusumano et al. (1998) by 0.82, to account for the effect of the PDS RT selection algorithm employed (see Sect. 1). The systematic uncertainty on this parameter can be estimated ±10%. Spectral fits have been performed in the 0.1–4 keV (LECS), 1.8–10.5 (MECS), 14–200 keV (PDS) energy bands.

4.1. Continuum shape

In Fig. 4 the result is shown, when a simple power-law model with photoelectric absorption is applied. The quality of the fit is rather poor ($\chi^2 = 262.6/122$ dof). The main deviations are due to: (a) an absorption feature starting at $E \simeq 0.7$ keV; (b) a prominent emission line with centroid energy $E \simeq 6.5$ keV; (c) a "bump" in the PDS band, peaking at energy $E \simeq 25$ keV. The residuals between 0.3 and 0.6 keV (immediately red wards the absorption feature) are systematically positive. In principle, this may be due to the emergence of a soft excess in this energy range. However, the recovery of the residuals to values consistent with zero below 0.3 keV leads to the suggestion the the above fea-

Table 1. BeppoSAX best-fit results. *wa* = photoelectric absorption from neutral matter; *po* = power-law; *px* = Compton reflection; *ga* = Gaussian line; *ed* = photoionization absorption edge; *bk* = broken power-law

Model	N_H $(10^{20}\ cm^{-2})$	Γ	R	E_c (keV)	σ (keV)	EW (eV)	E_{th} or E_{break} (keV)	τ or Γ_{soft}	$\chi^2/$ dof
`wa*po`	$1.55\pm^{0.14}_{0.13}$	1.70 ± 0.04							262.6/122
`wa*px`	1.9 ± 0.2	1.79 ± 0.04	$0.9\pm^{0.4}_{0.3}$						183.9/121
`wa*(px+ga)`	1.9 ± 0.2	1.80 ± 0.04	$0.8\pm^{0.4}_{0.3}$	$6.41\pm^{0.14}_{0.13}$	$0.2\pm^{0.3}_{0.2}$	$170\pm^{70}_{60}$			134.8/118
`wa*ed*(px+ga)`[a]	2.3 ± 0.3	1.87 ± 0.05	1.1 ± 0.4	$6.42\pm^{0.17}_{0.14}$	$0.3\pm^{0.3}_{0.2}$	$190\pm^{90}_{70}$	$0.77\pm^{0.06}_{0.05}$	$0.43\pm^{0.17}_{0.16}$	98.5/116
`wa*ed*(px+ga)`[b]	2.3 ± 0.3	1.86 ± 0.05	$1.0\pm^{0.6}_{0.4}$	$6.42\pm^{0.15}_{0.14}$	$0.3\pm^{0.3}_{0.2}$	$200\pm^{100}_{70}$	0.78 ± 0.06	$0.42\pm^{0.17}_{0.16}$	99.0/116
`wa*ed*(px+ga)`[c]	$1.5\pm^{1.7}_{1.4}$	$1.96\pm^{0.05}_{0.03}$	$0.6\pm^{1.0}_{0.0}$	$6.5\pm^{0.3}_{0.2}$	$0.5\pm^{1.0}_{0.4}$	$280\pm^{410}_{140}$	0.68 ± 0.03	$0.30\pm^{0.11}_{0.08}$	1396.4/1357
							$0.83\pm^{0.05}_{0.03}$	$0.13\pm^{0.05}_{0.07}$	
`wa*(bk+px+ga)`	1.4 ± 0.3	$1.87\pm^{0.13}_{0.06}$	$1.2\pm^{1.5}_{0.5}$	$6.42\pm^{0.18}_{0.17}$	$0.4\pm^{0.6}_{0.3}$	$240\pm^{170}_{90}$	2.2 ± 0.5	1.67 ± 0.07	133.6/116

[a] $\theta = 0$;

[b] $\theta = 30°$, "baseline model" in text.
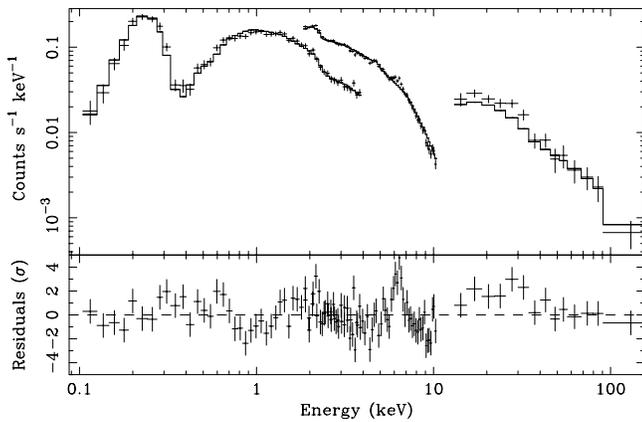
[c] fit on the ASCA data (see Sect. 5)

Fig. 4. Spectra and best-fit model (*upper panel*) and residuals in units of standard deviations (*lower panel*) when a simple power-law model with photoelectric absorption is applied

ture is simply the typical wavy residual produced by a mis-fit absorption edge (see e.g. Nandra & Pounds 1992). The BeppoSAX broadband allows to study simultaneously the whole spectral complexities expected on the basis of previous band-limited measures of this object and of the Seyfert 1s as a class (cf. Sect. 1). We have then defined a "baseline" model, where a Compton reflection component from a neutral slab (model `pexrav` in XSPEC, Magdziarz & Zdziarski 1995), an emission line and a photoionization absorption edge are superposed to the photoelectric absorbed power–law. The possibility that the reflecting matter is substantially ionized is not required by the data. The model depends on the heavy element abundance (which has been held fixed to the solar one), and on the angle between the normal to the slab and the line of sight ("inclination angle" θ). θ has been held fixed to 30° hereinafter (the best-fit value arising from a fit of the iron line profile with a relativistic model, see Sect. 4.2). The only free parameter in addition to the power-law model of the continuum is the relative normalization R between the reflected and the primary components (equal to 1 for an isotropic source, illuminating a plane-parallel

infinite slab). The best-fit R and Γ are basically unaffected, if one assumes that the reflector is seen face-on (*i.e.*: $\theta = 0°$). The "baseline" model yields a very good $\chi^2 = 99.0/116$ dof. The Table 1 reports the best-fit parameters and results.

It is worth noticing that no soft excess above the extrapolation of the high-energy power–law is required. A model, where one replaces the absorption edge with a continuous break of the primary power-law provides a much worse fit ($\chi^2 = 133.6/116$ dof) and leaves significant residuals in the 0.2–1.3 keV energy range. Moreover, the best-fit spectrum is convex (*i.e.*: $\Gamma_{soft} < \Gamma$), further demonstrating that no soft excess is present in the data. The inferred absorbing column density is consistent with the Galactic contribution along the line of sight as measured by Elvis et al. (1989, $N_{H_{Gal}} = 1.97 \times 10^{20}\ cm^{-2}$). The best–fit model and deconvolved spectra are shown in Fig. 5. The 0.1–2 keV, 2–10 keV and 20–100 keV fluxes are $\simeq 2.11 \times 10^{-11}$, 3.74×10^{-11} and $7.22 \times 10^{-11}\ erg\ cm^{-2}\ s^{-1}$, respectively. They correspond to rest frame luminosities of 5.80×10^{42}, 1.03×10^{43} and $1.99 \times 10^{43}\ erg\ s^{-1}$, respectively.

The unprecedented BeppoSAX energy coverage allows the simultaneous determination of the primary radiation steepness and of the Compton reflection intensity with the best accuracy ever achieved. In Fig. 6 the contour plot for the photon index versus the relative normalization between the reprocessed and primary components R is shown. The latter parameter is 1 if the reflection occurs in an infinite, plane-parallel slab and the primary source emits isotropically. Higher values are formally possible, and may be due to the geometry of the reflecting matter, covering more than 2π (e.g. in a concave or warped accretion disk), to an intrinsic anisotropy of the primary source, or to a delayed response of the reflecting matter to changes of the primary flux. At 90% level of confidence for two interesting parameters, the photon index is constrained between 1.81 and 1.91. R is consistent with a plane-parallel geometry of the reflecting matter (90% confidence interval between 0.6 and 1.6). Any cut-off of the intrinsic power-law is constrained to lay at energies higher then 150 keV (see Fig. 7). It is worth noticing that the statistical
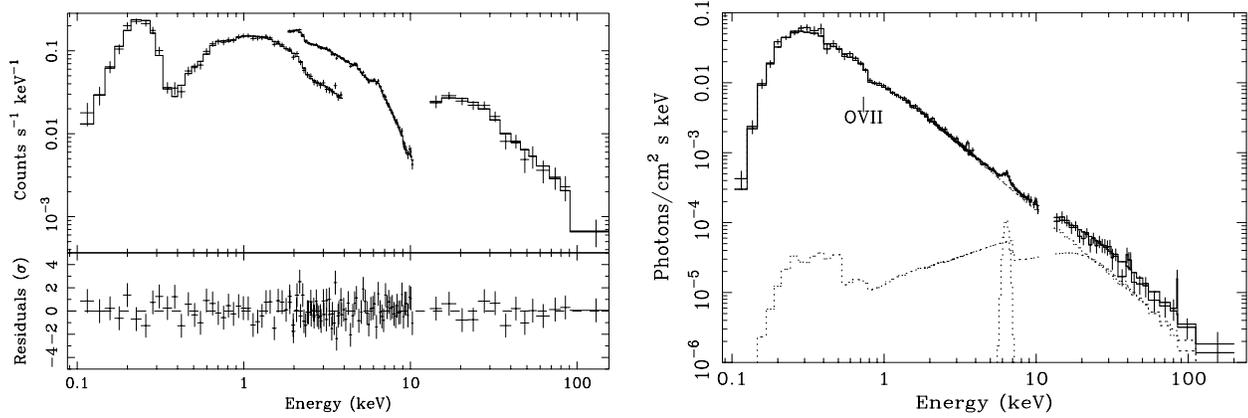
Fig. 5. *Left:* spectra and best-fit model (*upper panel*) and residuals in units of standard deviations (*lower panel*) when the "baseline" model is applied. *Right:* unfolded energy spectrum and best-fit model (solid lines). The direct and reflected continuum and the emission line are separately indicated with dotted lines. The location of the O VII photoionization absorption edge in the observers frame is labeled
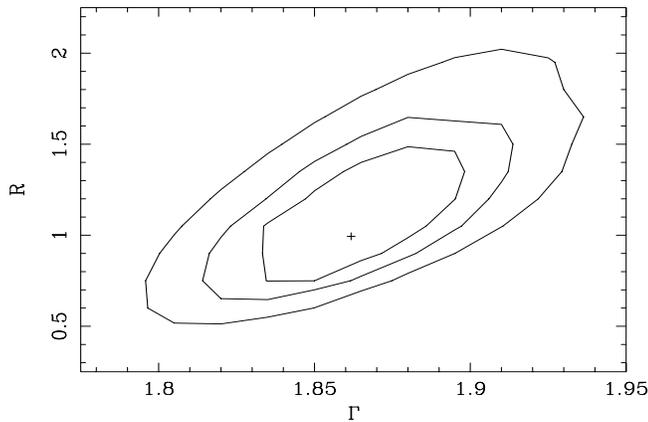

Fig. 6. Contour plot of the relative normalization between the primary and Compton reflected spectral components versus the intrinsic photon index, when the "baseline" model is employed. Iso-χ^2 curves are at 68%, 90% and 99% confidence level for two interesting parameters ($\Delta\chi^2 = 2.3$, 4.6 and 9.2)
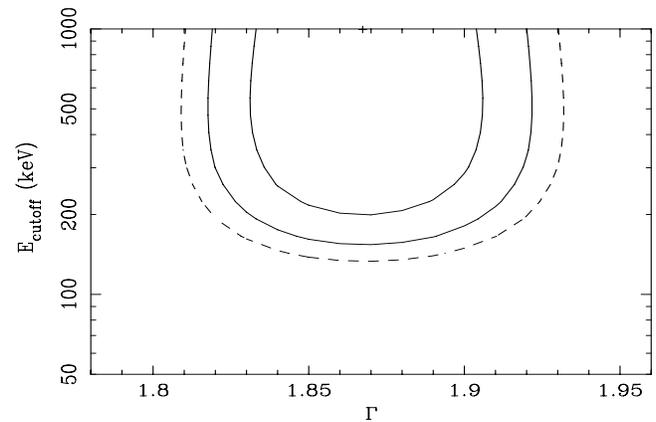
Fig. 7. Contour plot of the cutoff energy of the primary power-law component versus the photon index when the "baseline" model is employed

relative uncertainties on Γ and R are rather small, despite the strong correlation between the two parameters (note the strongly inclined contour plot in Fig. 7). For comparison, the single parameter 68% statistical errors ($\Delta\Gamma = 0.02$ and $\Delta R/R = 0.17$) are 4.5 and 3.5 times smaller than the ones obtained from the Ginga observations of the same Seyfert 1 (Nandra & Pounds 1994). It should however be noticed that the residual systematic uncertainties on the relative PDS to MECS normalization factor affect the accuracy of both these parameters, with additional uncertainties of about 1% and 30%, respectively.

Fig. 8. Contour plot of the intrinsic width versus the centroid energy of the iron line, when the "baseline" model is employed

4.2. On the K_α iron line

The centroid energy of the iron line is well consistent with Kα fluorescence from neutral iron. The line is broad if a simple broad Gaussian profile is used to describe it (see Fig. 8); the intrinsic width is comprised in the range 60–600 eV at 90% level of confidence for two interesting parameters (best-fit value $\simeq$
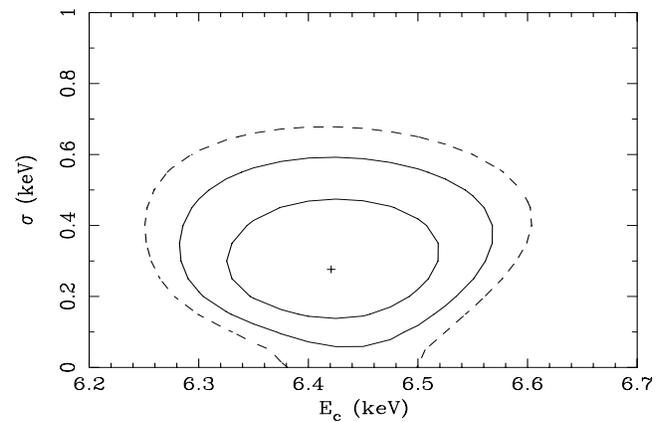
300 eV). We have tried also alternative parameterization of the line. Adding a further "narrow" line (*i.e.*: intrinsic width σ held fixed at zero) to the "baseline" model results in no improvement of the quality of the fit ($\Delta\chi^2 = 0$). Given the intrinsic width of the line and the agreement between the derived best–fit line
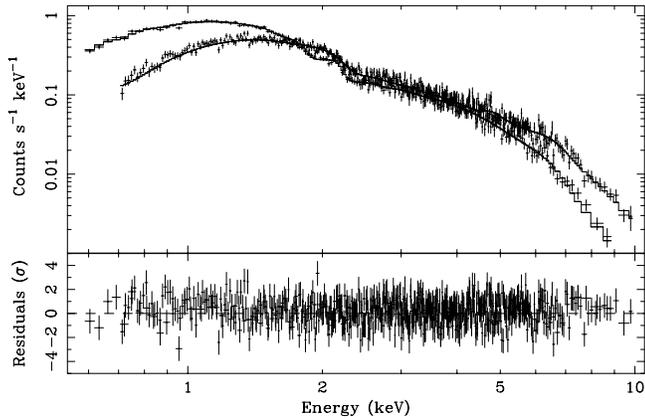
Fig. 9. Spectra and best-fit model (*upper panel*) and residuals in units of standard deviations (*lower panel*) when the modified BeppoSAX "baseline" model is applied to the January 1994 NGC 4593 ASCA observation. Only SIS1 and GIS3 data are shown for clarity

EW and the theoretical expectations if the line is produced in an X–ray illuminated relativistic accretion disk (Matt et al. 1992), we have tried to use a self-consistent model of line emission from a relativistic accretion disk (model `diskline` in XSPEC, Fabian et al. 1989). If all its parameters are allowed to be free, most of them are totally unconstrained. No further constraint comes from the ASCA data as well (Nandra et al. 1997). If it is assumed that the inner radius R_i of the emitting region is 6 gravitational radii ($R_G \equiv GM/c^2$); the emissivity law index is equal to -2.5 (Nandra et al. 1997); the inclination of the line and Compton reflection continuum emitting region is the same; and the line is neutral (*i.e.*: $E_c = 6.4$ keV); then $\theta = 32°\pm^{23}_{12}$, $\log(R_o) > 2.1$ and EW $= 240\pm^{70}_{60}$ eV. The quality of the iron line modeling ($\chi^2 = 98.9/114$ dof) is comparably good as for the broad Gaussian.

4.3. The warm absorber

In 12 out of 24 Seyfert galaxies observed by ASCA, absorption edges from ionized species of oxygen have been detected (Reynolds 1997), which have been interpreted as the imprinting of warm gas along the path from the nucleus and us. NGC 4593 is one of these objects, and the BeppoSAX observation confirms this outcome, thanks to the detection of an absorption edge with threshold energy $E_{th} = 0.78 \pm 0.06$ keV. The edge energy is consistent with the K-photoionization threshold energy of OVII. We have tried to give a qualitative characterization of the ionization and chemical structure of the absorbing matter, by tentatively including in the fit four absorption edges, with threshold energies held fixed to the values expected from OVII (0.739 keV), OVIII (0.871 keV), NeIX (1.196 keV) and NeX (1.362 keV). However, the available statistics is not good enough to give us significant constraints. Only the OVII edge yields a significant detection ($\tau_{OVII} = 0.32^{+0.17}_{-0.16}$), while only upper limits can be obtained for the other three edges ($\tau_{OVIII} < 0.22$, $\tau_{NeIX} < 0.05$, $\tau_{NeX} < 0.03$). Using CLOUDY (Ferland 1996), we have constructed a grid of self-consistent

models of the spectra transmitted through a ionized gas in thermal and ionization equilibrium, when the SED is the one observed in NGC 4593 (Santos-Lleó et al. 1995). They depend on the ionization parameter U (defined as the dimensionless ratio between the number of Hydrogen ionizing photons and the electron density of the gas), and the warm column density N_W. The fit is comparably good as the phenomenological description of the "baseline" model ($\chi^2 = 104.6/116$). The best-fit parameters of the warm absorbing matter are $N_W = (2.5\pm^{1.5}_{1.2}) \times 10^{21}$ cm^{-2} and $\log(U) = -0.7 \pm 0.3$. For a source with $\alpha_{ox} \simeq 1.20$, the best-fit U corresponds to a value of the more common $\xi \equiv L/n^2R \simeq$ a few. The continuum parameters are slightly affected ($\Gamma = 1.92 \pm 0.10$; $R = 1.3 \pm 0.5$), but remain consistent with the one of the "baseline" model within the statistical uncertainties.

5. Comparison with ASCA and ROSAT results

Nandra et al. (1997) detected with ASCA a weak (EW $= 90\pm^{40}_{30}$ eV) and narrow iron line, whose best-fit parameters are inconsistent with the ones corresponding to the "baseline" BeppoSAX best-fit model. We have therefore re-analyzed the ASCA observation to check the robustness of the iron line variability. ASCA (Tanaka et al. 1994) payload include a pair of Charged-coupled devices (SIS0 and SIS1, 0.57–9 keV) and a pair of gas scintillation proportional counters (GIS2 and GIS3, 0.7–10 keV). It observed NGC 4593 on January 9, 1994. Spectra have been extracted from the screened event files, which have been filtered according to standard criteria, using extraction radii of 2.30′, 3′ and 6′ for the SIS1, SIS0 and GIS, respectively. Net exposure times amount to 30 and 33 ks for the SIS and GIS, respectively. The spectra have been rebinned in order to have at least 20 counts per energy channel. Background spectra have been extracted from blank sky pointing event files, using the same extraction region in detector coordinates as the source. The same BeppoSAX "baseline" model has been applied to the spectra of all detectors simultaneously, except for the fact that ASCA is capable to resolve the OVII and OVIII absorption edges. The parameter R, which cannot be constrained by ASCA given the limited bandwidth of its instruments, has been forced to be comprised in the 90% confidence level range determined by BeppoSAX data, *i.e.*: 0.6–1.6. The time-averaged 2–10 keV flux in the ASCA observation is very close to that measured by BeppoSAX (F $\simeq 3.70 \times 10^{-11}$ erg s^{-1} cm^{-2}). No significant deviation exists between the ASCA and BeppoSAX best-fit parameters, with the exception of a slight steepening of the intrinsic power-law ($\Delta\Gamma = 0.10\pm^{0.10}_{0.07}$, cf. Table 1). In particular, the iron emission line best-fit parameters are consistent with the one obtained from the BeppoSAX data analysis within the statistical uncertainties and there is no evidence for a much weaker line in the ASCA data. It is worth noticing that no soft excess is required. The ASCA spectra and residuals against the best-fit are shown in Fig. 9.

Walter & Fink (1993) report the measure of a very steep ($\Gamma = 2.5$) intrinsic spectral index with ROSAT. However, their analysis does not take into account the possible contribu-

tion of a ionized absorber. We therefore reanalyzed the data of a pointed NGC 4593 ROSAT/PSPC observation, to compare BeppoSAX and ROSAT findings. The ROSAT observation was performed July 14 1992. The average spectrum was extracted, using a circular region about $2'$ radius around the source centroid. The background spectrum was extracted from a surrounding annulus of radii $4.'3$ and $7.'5$, after removing a $2'$ circular area around a weak serendipitous source at $\alpha_{2000} = 12^h 39^m 39^s.2$, $\delta_{2000} = -5°26'13''$. Total exposure time is 1261 s. Publicly available response matrices, appropriate for the epoch of the observation, were employed and spectral fit were performed in the energy range 0.1–2 keV, where these matrices are best calibrated. A simple power-law model with photoelectric absorption is an adequate description of the spectrum ($\chi^2 = 9/17$ dof), with best-fit parameters: $N_H = (2.1 \pm 0.5) \times 10^{20}$ cm^{-2}, $\Gamma = 2.13^{+0.19}_{-0.17}$, 0.1–2 keV flux $\simeq 1.26 \times 10^{-11}$ erg cm^{-2} s^{-1}. The intrinsic spectral index derived by ROSAT is indeed steeper than measured by BeppoSAX or ASCA, but by an amount much smaller than reported by Walter & Fink (1993). The soft excess above a $\Gamma = 1.86$ power-law is only 20% in flux against the 270% reported by these authors. The different energy band-passes in which the spectra are taken, or slight residuals misalignment in the cross calibration between ROSAT detectors and other missions (cf. Yaqoob et al. 1994; Iwasawa et al. 1998; Iwasawa et al. 1999) may easily account for this effect. Interestingly enough, no absorption edge is required by the ROSAT data despite the better effective area of the PSPC in comparison to the LECS (the energy resolution is comparable at 0.5 keV). The upper limit on the optical depth of a 0.77 keV absorption edge is 0.26. This might be suggestive of a long-term *positive* correlation between flux and warm absorber features, since the 0.1–2 keV flux is 60% in the ROSAT observation than in the BeppoSAX one. This aspect may be worth further investigation by future X-ray monitoring programs.

6. Discussion

The broadband (0.1–200 keV) X-ray spectrum of the Seyfert 1 galaxy NGC 4593 shows most of the typical features of its class. The continuum is well described by the superposition of a power-law primary component with $\Gamma \simeq 1.9$ and a Compton reflection component. The spectral index is broadly consistent both with Ginga (Nandra & Pounds 1994) and ASCA (Nandra et al. 1997) measurements, and close to the typical values observed in Seyfert 1s as a class (Nandra & Pounds 1994, Nandra et al. 1997). The best-fit nominal values on R is consistent with a slab geometry for the reflecting matter. The reflection component is therefore likely to originate in an X-ray illuminated relativistic accretion disk (AD), which subtends a $\simeq 2\pi$ solid angle from the nuclear source. This picture is consistent with the properties of the iron emission line. Its centroid energy is well consistent with Kα fluorescence from neutral or mildly ionized iron ($E_c = 6.42^{+0.15}_{-0.14}$). The line is moderately broad ($\sigma \simeq 0.3$). Fluorescence iron lines are expected to be produced, along with the Compton reflection continuum, in AD and broadened by the

combination of gravitational and Doppler effects if the photons undergo the effects of the gravitational potential of a supermassive black hole. The $\simeq 200$ eV EW is around the expectation values if the AD matter has nearly solar abundances, given the measured value of R (Matt et al. 1992). NGC 4593 does not suffer the iron overabundance problem that affects the relativistic iron line measure in some bright objects (among which the best studied case so far: MCG-6-30-15, Tanaka et al. 1995; see also Nandra et al. 1997) or to require a contribution from a narrow line component, which may originate in the molecular torus surrounding the nuclear environment in the unification scenario (Ghisellini et al. 1994; Krolik et al. 1994), and observed in several cases (Guainazzi et al. 1996; Weaver et al. 1997; George et al. 1998; Guainazzi et al. 1998a). The line properties can in principle constrain the location of the emitting region and the geometry of the AD. Fitting the iron line profile with a relativistic model allows us to constrain the inclination of the system ($\theta = 32°^{+23}_{-12}$), under the assumptions that the bulk of the iron line emitting region is neutral.

The combination of intermediate X-ray continuum and iron emission line properties is hence perfectly consistent with the standard picture for the production of high-energy radiation in the nuclear region of radio-quiet nearby AGN. The primary continuum, with the "canonical" $\Gamma = 1.9$ power-law index, is isotropically produced in the neighborhood of the nuclear supermassive black hole and reprocessed via Compton down scattering and fluorescence by an optically thick and geometrically thin Shakura-Sunyaev disk (Shakura & Sunyaev 1973), whose extension is much larger than the typical size of the primary continuum production region. The reprocessing matter does not exhibit any substantial ionization or deviation from cosmic abundances.

EXOSAT (Ghosh & Soundararajaperumal 1993; Santos-Lleó et al. 1994) observed a strong and remarkably variable soft excess. Its intensity was between 0 and 45% of the extrapolated high-energy flux in seven EXOSAT observations, when soft and intermediate X-rays were measured simultaneously. In EXOSAT data, it seems to exist no obvious correlation between the soft excess and the intermediate X-ray flux or spectral index (Santos-Lleó et al. 1994). Santos-Lleó et al. (1994) discuss the soft excess in terms of thermal emission from an accretion disc and conclude that the maximum temperature T_{max} should be ~ 210 eV. Such a disk blackbody component would be clearly detectable by the LECS (if not by the ASCA/SIS). If we add to the BeppoSAX "baseline" model the emission from a disc blackbody with temperature at the innermost disk radius $T = 100$ eV $= 0.488 T_{max}$ (Pringle 1981), its luminosity is $< 3 \times 10^{42}$ erg s^{-1}. A possible physical explanation for the disappearance of the soft excess may be a cooling of the disc temperature profile, which shifts T_{max} out of the BeppoSAX sensitive bandpass. Alternatively, the lack of soft excess detection could be simply due to the improved continuum determination, made possible by the broadband BeppoSAX spectral coverage. The 2–6 keV spectrum, against which Santos Lleó et al. (1994) measured the soft excess in EXOSAT data, was flatter than in our BeppoSAX baseline model ($< \Gamma_{EXOSAT} \simeq 1.73 >$). If one

fits the LECS/MECS data between 2 and 6 keV, one gets indeed $\Gamma \simeq 1.76$. Extrapolating this power-law in the 0.1–2 keV Bep-poSAX/LECS leaves a complex residual spectrum, with positive and negative wiggles, dominated by the OVII absorption feature. The interpretation of this residual spectrum in the broad EXOSAT/LE filters is not totally unambiguous. We conclude that the claimed soft excess might be simply an artifact, due to extrapolating the 2–6 keV spectrum into the low energy filter EXOSAT energy bandpass and/or to fitting a complex ionized absorber with the Galactic cold photoabsorption only. On the other hand, the lack of soft X-ray excess is in line with the lack of blue bump in this source (Santos-Lleó et al. 1994).

Another new result emerging from the BeppoSAX observation of NGC 4593 is the lack of any significant cutoff on the primary power-law, a lower limit on E_{cutoff} being $\simeq 150$ keV. This outcome is consistent with the measures of cutoff energies on individual sources available so far: NGC 4151 (70–270 keV, Zdziarski et al. 1995; Piro et al. 1998), IC4329A (240–900 keV Madejski et al. 1995), MCG-6-30-15 (100–390 keV; Guainazzi et al. 1999), and NGC 5548 (110–200 keV; Nicastro et al. 1999).

References

Barr P., Clavel J., Giommi P., Mushotzky R.F., Madjeski G., 1987, Proceeding Villa Olmo Meeting, AADA, Milano, p. 43
Boella G., Perola G.C., Scarsi L., 1997b, A&AS 122, 299
Boella G., Chiappetti L., Conti G., et al., 1997a, A&AS 122, 372
Cappi M., Mihara T., Matsuoka M., et al., 1996, ApJ 458, 149
Cusumano G., Mineo T., Guainazzi M., et al., 1998, A&A, submitted
Czerny B., Elvis M., 1987, ApJ 321, 305
Elvis M., Wilkes B.J., Lockman F.J., 1989, AJ 97, 777
Fabian A.C., Rees M.J., Stella L., White N.E., 1989, MNRAS 238, 729
Ferland, 1996, CLOUDY:90.01
Frontera F., Costa E., Dal Fiume D., et al., 1997, A&AS 122, 357
George I.M., Fabian A.C., 1991, MNRAS 249, 352
George I.M., Turner T.J., Netzer H., et al., 1998, ApJS 114, 73
Ghisellini G., Haardt F., Matt G., 1994, MNRAS 267, 743
Ghosh K.K., Soundararajaperumal S., 1993, A&A 273, 397
Grandi P., Guainazzi M., Mineo T., et al., 1997, A&A 325, L17
Guainazzi M., Mihara T., Otani C., Matsuoka M., 1996, PASJ 48, 781
Guainazzi M., Nicastro F., Fiore F., et al., 1998a, MNRAS 301, L1

Guainazzi M., Piro L., Capalbi M., et al., 1998b, A&A 339, 337
Guainazzi M., Matt G., Molendi S., et al., 1999, A&A 341, L27
Haardt F., Fossati G., Grandi P., et al., 1998, A&A 340, 35
Holt S.S., Mushotzky R.F., Becker R.H., et al., 1980, ApJ 241, L13
Iwasawa K., Fabian A.C., Reynolds C.S., et al., 1996, MNRAS 282, 1038
Iwasawa K., Brandt N.W., Fabian A.C., 1998, MNRAS 293, 251
Iwasawa K., Fabian A.C., Nandra K., 1999, MNRAS, submitted
Johnson W.N., Grove J.E., Kinzer R.L., et al., 1993, AAS, 183, 640
Krolik J.H., Madau P., Zycki P.T., 1994, ApJ 420, L57
Lampton M., Margon B., Bowyer S., 1976, ApJ 208, 177
Laor A., Fiore F., Elvis M., Wilkes B.J., McDowell J.C., 1997, ApJ 477, 93
Madejski G.M., Zdziarski A.A., Turner T.J., et al., 1995, ApJ 438, 672
Magdziarz P., Zdziarski A.A., 1995, MNRAS 273, 837
Malizia A., Bassani L., Malaguti G., et al., 1997, Mem. Soc. Astron. Ital. 68, 145
Manzo G., Giarrusso S., Santangelo A., et al., 1997, A&AS 122, 341
Matt G., Perola G.C., Piro L., 1991, A&A 247, 25
Matt G., Perola G.C., Piro L., Stella L., 1992, A&A, 257, 63
Mushotzky R.F., 1984, Adv. Sp. Res. 3, 10
Mushotzky R.F., Done C., Pounds K.A., 1993, ARA&A 31, 717
Nandra K., Pounds K., 1992, Nat 359, 215
Nandra K., Pounds K., 1994, MNRAS 268, 405
Nandra K., George I.M., Mushotzky R.F., et al., 1997, ApJ 488, L91
Netzer H., 1996, ApJ 473, 781
Nicastro F., Elvis M., Fiore F., Perola G.C., 1998, ApJ, in press (astroph/9808316)
Nicastro F., Piro L., Grandi P., et al., 1999, ApJ, submitted
Parmar A.N., Martin D.D.E., Bavdaz N., et al., 1997, A&AS 122, 309
Perola G.C., Piro L., Altamore A., et al., 1986, MNRAS 306, 508
Piro L., Yamauchi M., Matsuoka M., 1990, ApJ 360, L35
Piro L., Balucińska-Church M., Fink H.H., et al., 1997, A&A 319, 74
Piro L., Feroci M., Grandi P., et al., 1998, In: Scarsi L., Bradt H., Giommi P., Fiore F. (eds.) Proceedings of the Symposium: The active X–ray sky: first results from Beppo-SAX and RXTE, in press
Pounds K., Nandra K., Stewart G.C., et al., 1990, Nat 344, 132
Pringle J.E., 1981, ARA&A 19, 137
Puchnarewicz E.M., Mason K.O., Romero-Colmenero E., et al., 1996, MNRAS 281, 1243
Reynolds C.S., 1997, MNRAS 286, 513
Santos Lleó M., Clavel J., Barr P., et al., 1994, MNRAS 270, 580
Santos Lleó M., Clavel J., Barr P., et al., 1995, MNRAS 274, 1
Shakura N.I., Sunyaev R.A., 1973, A&A 24, 337
Tanaka Y., Inoue H., Holt S.S., 1994, PASJ 46, L37
Tanaka Y., Nandra K., Fabian A.C., et al., 1995, Nat 375, 659
Turner T.J., Pounds K.A., 1989, MNRAS 232, 463
Turner T.J., Weaver K.A., Mushotzky R.F., 1993, ApJ 412, 72
Yaqoob T., Serlemitsos P. Mushotzky R.F., 1994, PASJ 46, 173
Walter R., Fink H.H., 1993, A&A 274, 105
Weaver K.A., Yaqoob T., Mushotzky R.F., et al. 1997, ApJ 474, 675
Zdziarski A.A., Johnson W.N., Done C., Smith D., McNaron-Brown K., 1995, ApJ 438, L63